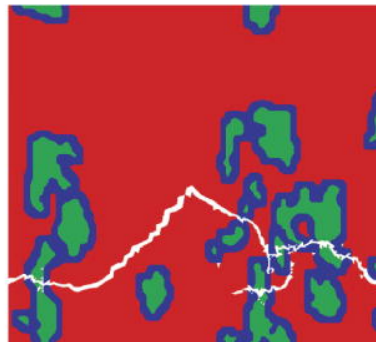




VOLUME 39, Issue 2
<http://www.elsevier.com/locate/commatsci>

APRIL 2007

COMPUTATIONAL
MATERIALS
SCIENCE



Editors:
H. DREYSSÉ
S. SCHMAUDER

Available online at

ScienceDirect
www.sciencedirect.com

ISSN 0927-0256

This article was originally published in a journal published by Elsevier, and the attached copy is provided by Elsevier for the author's benefit and for the benefit of the author's institution, for non-commercial research and educational use including without limitation use in instruction at your institution, sending it to specific colleagues that you know, and providing a copy to your institution's administrator.

All other uses, reproduction and distribution, including without limitation commercial reprints, selling or licensing copies or access, or posting on open internet sites, your personal or institution's website or repository, are prohibited. For exceptions, permission may be sought for such use through Elsevier's permissions site at:

<http://www.elsevier.com/locate/permissionusematerial>

A potential for simulating the atomic assembly of cubic elements

X.W. Zhou ^{a,*}, H.N.G. Wadley ^b

^a Department of Materials Science and Engineering, 116 Engineer's Way, University of Virginia, Charlottesville, Virginia 22904-4745, United States

^b Department of Materials Mechanics, 7011 East Avenue, Sandia National Laboratories, Livermore, California 94551-0969, United States

Received 24 May 2006; received in revised form 1 July 2006; accepted 3 July 2006

Abstract

Molecular dynamics simulations using Stillinger–Weber potentials have been widely used to study the growth of diamond-cubic materials since these potentials are easily parameterized to ensure that the diamond-cubic structure has the lowest cohesive energy. However, Stillinger–Weber potentials can only be used to model cubic crystals with the diamond-cubic structure. Here we generalize the Stillinger–Weber potential formalism and explore its application to other cubic crystal structures. Parameterization of this modified Stillinger–Weber potential is exemplified by developing potentials for four elements: Si (diamond-cubic), Ni (face-centered-cubic), Fe (body-centered-cubic), and Po (simple-cubic). The parameterized potentials predict well the cohesive energy and lattice constants of each element. Molecular dynamics simulations are used to test the ability of the potentials to simulate the crystalline assembly of these materials from their atomic vapor. Defects are found in the films grown under kinetically constrained conditions.

© 2006 Elsevier B.V. All rights reserved.

Keywords: Molecular dynamics simulations; Interatomic potential; Vapor deposition; Thin films

1. Introduction

The crystalline structures of thin films are essential to a variety of applications. For example, solid state transistors are made from diamond-cubic (dc) Si or zinc-blende (zb) GaAs thin films [1]. Many light emitting diodes, ultraviolet detectors, and ultrahigh power devices are made from wurtzite (wz) and zb GaN films [2–4]. The magneto transport properties [5,6] of magnetic tunnel junctions [7,8] used for magnetic field sensing [9–11] and magnetic random access memory [7,12] were also found to significantly improve when a B1 crystalline MgO tunnel barrier layer is used [13]. Each of these thin films is grown by vapor deposition processes, and device properties can be highly sensitive to the lattice defects trapped in the films. The lattice defects present in the deposited films are determined by the growth conditions. Atomistic simulation techniques, such as molec-

ular dynamics, are beginning to allow visualization of the atomic scale assembly of thin films and identification of the processes that lead to defect trapping [14–17].

Molecular dynamics simulations of atomic scale structure evolution require interatomic potentials to calculate the forces for an assemble of atoms or ions. The potentials are also used in molecular statics simulations to calculate the energy barriers impeding atom reconstructions and these energy barriers are in turn used in kinetic Monte Carlo simulations of the kinetic assembly of atomic structures. Embedded atom method potentials [14,18] developed for close-packed metal structures [19] have been widely used to simulate the crystalline growth of metal and metallic multilayered thin films [14,15,17]. However, the embedded atom method addresses only radially dependent interatomic forces and is not suitable for the study of the more complicated crystal structures encountered in semiconductors, nitrides, and oxides where the bonding has a significant directional character. Many angularly dependent potential formats have been proposed for these complicated structures, and those based upon the Stillinger–Weber (SW) [20] and Tersoff [21–24] formats have been widely used.

* Corresponding author. Tel.: +1 295 294 2851; fax: +1 295 294 3410.
E-mail addresses: xzhou@sandia.gov, xiaowang.zhou@gmail.com (X.W. Zhou).

Recent analysis of both the SW and Tersoff potentials [25] indicates that the SW potential can be easily fitted to the lattice constant, the cohesive energy, and elastic constants of both dc and zb crystal structures while simultaneously predicting less stable cohesive energies for other phases. This is a direct result of the potential formulism. In SW potentials, the cohesive energy, E_c , is expressed as the sum of a two-body (pairwise) interaction, Φ , and a three-body (angularly dependent) interaction, Θ ($E_c = \Phi + \Theta$) [20]. The three-body, Θ term is designed to vanish when the bond angle equals that of the dc or zb crystal structures. The two-body, Φ term then uniquely describes the cohesive energy, the lattice constant, and the bulk modulus of the equilibrium dc or zb phase. Because all other phases always have different bond angles from that of the dc or zb crystal structure, the lowest energy is ensured for the dc or zb phase by simply designing the three-body Θ term so that it increases very rapidly as the bond angle deviates from that of the dc or zb structure. During crystal growth simulations, this feature of the potential correctly destabilizes surface structure abnormalities and SW potentials therefore usually simulate the crystalline growth of dc and zb structures quite well [26–29].

The Tersoff potential appears to offer better generality since it facilitates fitting to the lattice constant, the cohesive energy, and the elastic constants of an equilibrium dc or zb crystal as well as to the lattice constant and the cohesive energy of many other higher energy (metastable) crystalline phases. However, this improved transferability to other phases unfortunately makes the potential more difficult to parameterize for most material systems of interest. If the potential is not sufficiently well parameterized, it can incorrectly over-stabilize metastable configurations, leading to their (erroneous) nucleation during thin film growth. These configurations are often retained during simulations, and can incorrectly result in the growth of amorphous structures. On the other hand, few of the well parameterized Tersoff potentials [30,31] were demonstrated to predict the crystalline growth of compound films (e.g., of GaN [32]) under reasonable deposition conditions.

The relative ease of parameterization of SW potentials and their satisfactory prediction of the epitaxial growth of dc and zb crystals have made them a preferred choice for growth simulations for materials that condense with these crystal structures [26–29]. However, the growth of other compounds (such as some binary metal oxides) with different equilibrium crystal structures (e.g., B1 and B2) cannot be successfully modeled using this potential. A generalized SW potential formulism for these cubic structures would therefore be useful. One approach to modify SW potentials for wz crystal structure has been proposed [33]. Here we show that a similar approach can be used to modify an elemental SW potential so that it can be used to simulate the vapor phase assembly of dc, simple-cubic (sc), face-centered-cubic (fcc), and body-centered-cubic (bcc) crystal films. The extension of this modified SW potential format to AB cubic compound systems (with

B1, B2, or B3 crystal structures) is discussed in a subsequent paper [34].

2. Structural parameters of cubic crystals

Our goal is to modify a SW potential to facilitate its use for any of the cubic (dc, sc, fcc, and bcc) crystals. We begin by defining several structural parameters for a crystal structure. The ratio $\xi_i = r_i/r_1$ measures the radius of the i th nearest neighbor shell, r_i , to that of the nearest neighbor shell, r_1 . A coordination number, Z_i , represents the number of atoms in the i th nearest neighbor shell. A volume conversion factor, F , relates the atomic volume, V , to the nearest neighbor distance, r_1 , by the relation $V = F \cdot r_1^3$. Values of these parameters (up to the second nearest neighbor shells) are tabulated in Table 1 for the four cubic crystal structures.

Angular independent potentials always predict that densely packed lattices such as fcc or bcc structure have the lowest cohesive energies (eV/atom). This is because these structures form a maximum number of short bonds (the fcc structure has 12 nearest neighbors, and the bcc structure has eight nearest and six next nearest neighbors with very close distances). To use an angular dependence to reorder the relative stability of different phases, the bond angles in different structures must be characterized. The bond angle formed at atom i by its two neighbors j and k is denoted as θ_{jik} . All possible cosine values of the bond angles, θ_{jik} , and the bond angle degeneracy, N_{jik} , are listed in Table 2 for the four cubic crystals.

Table 1
Structural parameters for dc, sc, bcc and fcc crystals

Structures	Relative atom spacing $\xi_i = r_i/r_1$		Coordination Z_i		F factor
	$i = 1$	$i = 2$	$i = 1$	$i = 2$	
dc	1	$\sqrt{8/3}$	4	12	$8/\sqrt{27}$
sc	1	$\sqrt{2}$	6	12	1
fcc	1	$\sqrt{2}$	12	6	$1/\sqrt{2}$
bcc	1	$2/\sqrt{3}$	8	6	$4/\sqrt{27}$

Table 2
Cosine values of the bond angle, θ_{jik} , and their degeneracy, N_{jik} , for dc, sc, bcc and fcc crystals

Structures	$\cos \theta_{jik}$	Number of bond angles
dc	$-1/3$	6
sc	-1	3
	0	12
fcc	-1	6
	$-1/2$	24
	0	12
	$1/2$	24
bcc	-1	4
	$-1/3$	12
	$1/3$	12

Table 2 indicates that in a dc structure, each atom has six bond angles with an identical value of $\cos\theta = -1/3$. Other cubic crystals have multiple values of $\cos\theta$.

3. The Stillinger–Weber potential

In the original SW potential [20], the cohesive E_c of an atomic assembly is written as

$$E_c = \frac{1}{2N} \sum_{i=1}^N \sum_{j=i_1}^{i_N} \phi(r_{ij}) + \frac{1}{2N} \sum_{i=1}^N \sum_{j=i_1}^{i_N} \left[\left(\sum_{\substack{k=i_1 \\ k \neq j}}^{i_N} u(r_{ik}) \cdot g(\cos\theta_{jik}) \right) \cdot u(r_{ij}) \right] \quad (1)$$

where the first and the second terms on the right hand side of Eq. (1) represent respectively the two-body (Φ) and the three-body (Θ) contributions as discussed above. In Eq. (1), N is the total number of atoms in the system, i_1, i_2, \dots, i_N represents a list of all the neighbors of atom i (including image atoms in the periodic computational cell), $\phi(r_{ij})$ is a pair interaction energy between atoms i and j separated by a distance r_{ij} , $u(r)$ is a positive pair function used in the angular interaction, and $g(\cos\theta_{jik})$ is a function of the cosine of the bond angle.

The radially dependent functions $\phi(r)$ and $u(r)$ are expressed in the form

$$\phi(r) = A \cdot S \left(\frac{\sigma}{r} \right)^4 \exp \left(\frac{\sigma}{r - r_c} \right) - A \cdot \exp \left(\frac{\sigma}{r - r_c} \right) \quad (2)$$

and

$$u(r) = C \cdot \exp \left(\frac{\gamma}{r - r_{uc}} \right) \quad (3)$$

where $r_c = r_{uc}$, and $A, S, C, \sigma, \gamma, r_c$ represent six fitted parameters. It can be seen that functions $\phi(r)$ and $u(r)$ smoothly decay to zero at $r = r_c$, the cutoff distance of the two functions. The original SW potential is a nearest neighbor potential, so r_c is therefore set to be less than the second nearest neighbor distance in the dc or zb structure. In that case, i_1, i_2, \dots, i_N is a list of the nearest neighbors of atom i . The natural incorporation of a smooth cutoff is an important property of the SW potential.

The angular dependent function $g(\cos\theta)$ is written as

$$g(\cos\theta) = \left(\cos\theta + \frac{1}{3} \right)^2 \quad (4)$$

Eq. (1) indicates that for SW potential, the cohesive energy of a material is the sum of two pairwise terms $\phi(r_{ij})$ and $u(r_{ij})$, with $u(r_{ij})$ multiplied by an angular term $\sum_{\substack{k=i_1 \\ k \neq j}}^{i_N} u(r_{ik}) \cdot g(\cos\theta_{jik})$. This, at a first sight, appears very similar to the Tersoff potential [21–24]. However, in the Tersoff potential, the $\phi(r)$ term corresponds to a repulsive energy and the $u(r)$ corresponds to an attractive energy. As a result, the value of $u(r)$ is always negative and the

angular term is not equal to zero in equilibrium structures. In contrast, the $\phi(r)$ used in Eq. (1) is a complete pair interaction energy that includes both repulsive and attractive contributions. In addition, the $u(r)$ term is always positive. It can be seen that for a dc crystal where all bond angles satisfy $\cos\theta = -1/3$, the angular term becomes zero and the cohesive energy is entirely defined by the pair potential $\phi(r)$. When the bond angle deviates from the $\cos\theta = -1/3$ condition in other structures, Eq. (1) introduces a positive angular energy addition to the negative pair energy. As a result, the magnitude of the negative cohesive energy for other structures can always be made smaller than that of the dc structure provided that the value of $u(r_{ij})u(r_{ik})$ is made sufficiently large.

4. Modified Stillinger–Weber potential

For efficient computations, a short-ranged potential is sought. The angular term is therefore chosen to include only the nearest neighbor interactions. However, the pair energy cutoff distance is constrained by the requirement for a smooth cohesive energy dependence upon lattice constant relationship. For dc, sc, and fcc structures where the radius of the next nearest neighbor shell is significantly longer than that of the nearest neighbor shell (with ratio $\xi_2 \geq 1.414$, Table 1), the potential function can be smoothly cut off within the next nearest neighbor shell. As a result, potentials that involve only the nearest neighbor interactions can be satisfactory used for these crystals. However, in a bcc structure, the radius of the next nearest neighbor shell is very close to that of the nearest neighbor shell (with ratio $\xi_2 \approx 1.155$). The cutoff of the potential within the next nearest neighbor shell then results in an unphysically steep potential function between the equilibrium bond length and the cutoff distance. For bcc structures, it is necessary to consider both the nearest and the next nearest neighbor two-body interactions.

Two simple modifications can effectively extend the original SW potential to sc, fcc, and bcc structures. First, the interaction range of the pair potential can be allowed to extend beyond the nearest neighbor distance as required by the bcc crystal, while the angular interaction is restricted to the nearest neighbors for simplicity. This modification is incorporated when r_c and r_{uc} used in Eqs. (2) and (3) are treated as separate parameters such that $r_c > r_2$ and $r_{uc} < r_2$. Secondly, the g function can be modified so that it has a value of zero whenever a bond angle is equal to a bond angle in the appropriate equilibrium phase (dc, sc, fcc, or bcc). When the bond angle deviates from the ones in the equilibrium phase, the g function can be designed to rapidly increase.

In the original SW potential, the $g(\cos\theta)$ function quadratically minimizes to zero when the bond angle satisfies the dc structure constraint, $\cos\theta = -1/3$. The sc, fcc, and bcc crystals all have multiple bond angles as shown in Table 2. The idea of the g function of the original SW potential, however, can be applied to each of these crystals

Table 3
Angular function parameters for dc, sc, bcc and fcc crystals

Structures	M	n	$x_{\min,n}$	$x_{\max,n}$	$\cos \theta_n$	χ_n	$g_{o,n}$
dc	1	1	-1.00000	1.00000	-0.33333	1.0	0.00000
sc	3	1	-1.00000	-0.75000	-1.00000	1.0	0.00000
		2	-0.75000	-0.50000	-0.50000	-1.0	0.12500
		3	-0.25000	1.00000	0.00000	1.0	0.00000
fcc	7	1	-1.00000	-0.87500	-1.00000	1.0	0.00000
		2	-0.87500	-0.62500	-0.75000	-1.0	0.03125
		3	-0.62500	-0.37500	-0.50000	1.0	0.00000
		4	-0.37500	-0.12500	-0.25000	-1.0	0.03125
		5	-0.12500	0.12500	0.00000	1.0	0.00000
		6	0.12500	0.37500	0.25000	-1.0	0.03125
		7	0.37500	1.00000	0.50000	1.0	0.00000
bcc	5	1	-1.00000	-0.83333	-1.00000	1.0	0.00000
		2	-0.83333	-0.50000	-0.66667	-1.0	0.05556
		3	-0.50000	-0.16667	-0.33333	1.0	0.00000
		4	-0.16667	0.16667	0.00000	-1.0	0.05556
		5	0.16667	1.00000	0.33333	1.0	0.00000

by simply requiring that the $g(\cos \theta)$ function quadratically minimizes to zero at all of the possible bond angles in each structure. The existence of the multiple values of $\cos \theta$ in a given structure then defines multiple local quadratic functions. A smooth $g(\cos \theta)$ function can then be obtained by splining all these local quadratic functions. A splined $g(\cos \theta)$ function that achieves this objective can be written as

$$g(\cos \theta) = g_{o,n} + \chi_n (\cos \theta - \cos \theta_n)^2, \quad x_{\min,n} \leq \cos \theta < x_{\max,n},$$

$$n = 1, 2, \dots, M \quad (5)$$

where $g_{o,n}$, χ_n , $\cos \theta_n$, $x_{\min,n}$, $x_{\max,n}$ and M are parameters. A proposed set of values for these parameters is presented in Table 3 for the four cubic crystal structures.

The g functions defined by Eq. (5) and the coefficients of Table 3 are plotted in Fig. 1 for the four crystals. It can be seen that these g functions guarantee that the angular terms in Eq. (1) drop to zero for the equilibrium structures, and a positive energy adjustment is introduced when the bond

angles deviate from the ones defined by the equilibrium crystal.

5. Potentials for silicon, polonium, iron and nickel

At ambient temperature, Si, Po, Fe and Ni have dc, sc, bcc and fcc equilibrium crystal structures respectively. These elements can therefore be used to test the model potential format suggested above. The potential parameters of these elements were determined by fitting the potential predictions of the properties of each equilibrium crystal structure to those obtained from either experiments [35,36] or ab initio calculations [37]. Fitting of the potential is facilitated by analytical relations between material properties and the free parameters of the potential. Relations for cohesive energy, Eq. (A.1), lattice constant, Eq. (A.2), bulk modulus, Eq. (A.3), and shear moduli, Eq. (B.8), are summarized in the Appendices. It should be noted that when Eqs. (A.1)–(A.3) are satisfied, the cohesive energy, lattice constant, and bulk modulus for the equilibrium phase are exactly predicted. However, it has been found that such a parameterization often results in cohesive energy vs. lattice constant curves with multiple energy minima. Two factors contribute to this. First, the pair function specified by Eq. (2) may oscillate if the parameters are not properly chosen. Secondly, even when the parameters ensure that Eq. (2) does not oscillate, the cohesive energy may still have several minima due to superimposition of the nearest and the next nearest interactions that coexist in some structures. We found that no oscillatory behavior occurred for any of the four structures of each element (i.e., dc Si, sc Si, fcc Si, bcc Si, ...) as long as the parameter $S \ll A$. Under this additional $S \ll A$ constraint, only two of the three properties (cohesive energy, lattice constant, bulk modulus) can be exactly fitted. As structure evolution during growth is largely controlled by cohesive energy and lattice constant, our parameterization was carried out to

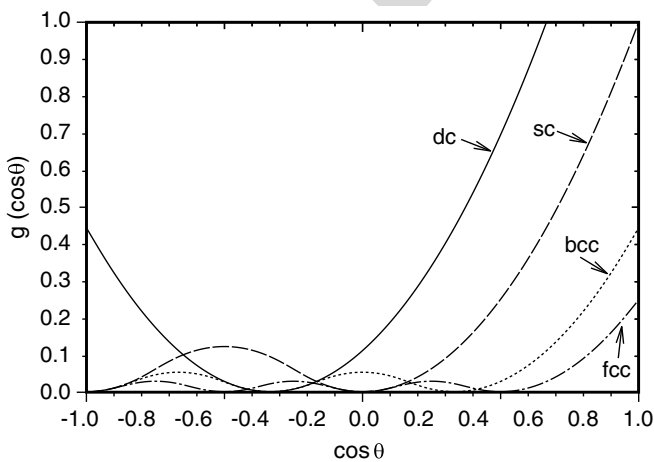


Fig. 1. g functions for four structures: dc, sc, fcc, and bcc.

exactly fit cohesive energy and lattice constant under the constraint $S \ll A$. This was performed by slowly adjusting the target value of the bulk modulus until the potential determined from Eqs. (A.1)–(A.3) predicted smooth cohesive energy vs. lattice constant curves for all four structures of each element.

It should also be noted that Eq. (B.8) can be used to determine the value of $u(r_1)$ by optimizing the prediction of the elastic shear moduli. However, while the parameterization procedure described above gives the best predictions for the properties of the equilibrium phase, it does not ensure that the equilibrium phase has the lowest cohesive energy. The lowest energy equilibrium phase can only be obtained by destabilizing the other phases using the u function. In general, a larger value of $u(r_1)$ more significantly destabilizes the other phases. In our parameterization, the value of $u(r_1)$ was chosen to predict the lowest energy for the equilibrium phase. Once this was satisfied, Eq. (B.8) was then used to improve the prediction of the shear moduli of the equilibrium phase.

After $u(r_1)$ has been determined, there is still remaining freedom between the γ and C parameters at a chosen value of r_{uc} . The function u increases as r decreases and therefore phases (other than the equilibrium crystal) that have shorter bond length can always be more effectively destabilized. A large value of r_{uc} helps extend the targeted phases for destabilization to a large bond length. A small γ increases the value of the function u when r is close to r_{uc} . As a result, a large r_{uc} and a small γ tend to more effectively destabilize phases with relatively long bond lengths. These parameters therefore sensitively affect the result of vapor deposition simulations. Iterations were thus carried out to select values for these parameters that

resulted in crystalline growth for all the equilibrium crystals.

Using the insights discussed above, proposed parameters to fully define the interatomic potentials for the four elements were determined and are listed in Table 4. The cohesive energy, lattice constant, and elastic moduli predicted by the potentials are compared with the target values (either experimental or ab initio data) in Table 5.

In Table 4, the parameter C for (bcc) Fe is zero. For the four elements we tested, only Fe did not require the angular dependent term for its equilibrium phase (bcc) to be the lowest cohesive energy phase in the modified SW potential formalism. Table 5 shows that the potentials predict the exact cohesive energies and lattice constants for the equilibrium phase of each of the four elements. The potential also predicts the exact bulk moduli for Si and Po, but the bulk moduli of Fe and Ni are not well predicted primarily due to the oscillatory behavior of the pair function formats, Eqs. (2) and (3).

Molecular statics methods were used to calculate the relaxed bulk structures and energies of the metastable cubic crystal phases for the four elements. The results are summarized in Tables 6 and 7 for the cohesive energy and the nearest neighbor distance respectively.

Table 6
Cohesive energy E_c (eV/atom) of various phases for Si, Po, Fe, and Ni

Element/structure	dc	sc	bcc	fcc
Si	-4.670	-4.138	-4.153	-4.036
Po	-0.584	-1.463	-0.845	-0.783
Fe	-1.396	-2.255	-4.320	-4.196
Ni	-1.469	-2.225	-4.310	-4.450

Table 4
Parameters for the Stillinger–Weber potentials for Si (dc), Po (sc), Fe (bcc), and Ni (fcc)

Element	A (eV)	S	C (eV ^{1/2})	σ (Å)	γ (Å)	r_c (Å)	r_{uc} (Å)
Si	15.31575	0.53734	7.72918	2.12986	2.66233	3.83881	3.83881
Po	9.21497	0.95525	13.71680	2.87141	3.44569	4.63726	4.63726
Fe	12.20092	0.23130	0.00000	3.15078	3.78094	4.05195	2.86216
Ni	9.499273	1.65683	2.77832	1.86519	2.23823	3.51897	3.51897

Table 5
Cohesive energy E_c , lattice constant, a , bulk modulus, B , elastic constants, C_{11} , C_{12} , and C_{44} , for Si (dc), Po (sc), Fe (bcc), and Ni (fcc)

Element	Data type	Cohesive energy E_c (eV/atom)	Lattice constant a (Å)	Elastic constants (eV/Å ³)			
				B	C_{11}	C_{12}	C_{44}
Si	Predicted	-4.670	5.431	0.612	1.006	0.415	0.678
	Target [35]	-4.670	5.431	0.612	1.036	0.400	0.498
Po	Predicted	-1.463	3.280	0.352	1.056	0.000	0.266
	Target [36]	-1.463	3.280	0.352	0.706	0.175	0.266 ^a
Fe	Predicted	-4.320	2.866	2.108	2.809	1.757	1.757
	Target [35]	-4.320	2.866	1.054	1.413	0.875	0.725
Ni	Predicted	-4.450	3.520	2.820	4.487	1.987	2.225
	Target [35,37]	-4.450	3.520	1.128	1.541	0.922	0.779

^a Deduced assuming anisotropic ratio of unity.

Table 7

The nearest neighbor distance r_1 (Å) of various phases for Si, Po, Fe, and Ni

Element/structure	dc	sc	bcc	fcc
Si	2.352	2.668	2.864	2.991
Po	3.533	3.280	3.657	3.798
Fe	2.604	2.302	2.482	2.597
Ni	2.493	2.488	2.373	2.489

Table 6 indicates that the equilibrium (dc) Si, (sc) Po, (bcc) Fe, and (fcc) Ni phases all have the lowest cohesive energies compared with the other three cubic phases.

6. Molecular dynamics simulations

The potentials parameterized above were used in molecular dynamics methods [14,15] to simulate the growth of the four elements by condensing their vapor on their close-packed equilibrium crystal surfaces. A deposition temperature of 650 K, an adatom energy of 1.0 eV, an adatom incident direction normal to the surface, and a growth rate of 0.5 nm/ns were used for the simulations.

The atomic configurations obtained after 2000 ps of condensation are displayed in Fig. 2(a)–(d) for the (100)Si, (111)Po, (110)Fe and (111)Ni surfaces respectively. It can be seen that all the elements developed crystalline film structures during growth simulations even though the adatoms arrived at the surface at random locations. This further verifies that the potentials correctly captured the lowest energy for the equilibrium phases with respect to any of the other configurations that were not considered during potential parameterizations.

Si films are known to form amorphous structures at low growth temperatures and the crystallinity of Si films improve with increasing growth temperatures [38]. Fig. 2(a) shows that a high quality dc crystalline Si film can be obtained from molecular dynamics simulations at a relatively high growth temperature of 650 K, a relatively high adatom energy of 1.0 eV, and at the accelerated growth rate of 0.5 nm/ns. This is in good agreement with other molecular dynamics simulations of Si vapor deposition [27].

The structures shown in Fig. 2(b)–(d) indicate that Po, Fe and Ni films all have crystalline structures, consistent with the simulated conditions (a growth temperature of 650 K, an adatom energy of 1.0 eV, and a rate of 0.5 nm/ns). No twins are observed for the Po and Fe films shown in Fig. 2(b) and (c). However, extensive growth twinning can be seen in Fig. 2(d) for the Ni film. During the growth of the fcc Ni in the [111] direction, the stacking sequence is ABCABC... Adatoms that condense on an A plane can fall on either B or C sites with almost an equal probability. As a result, growth twins are easily formed [39]. We also noted that the relatively rough Ni surface seen in Fig. 2(d) is consistent with the roughness of Ni surfaces observed in molecular dynamics simulations of Ni/Cu multilayer growth using embedded atom method potentials [17].

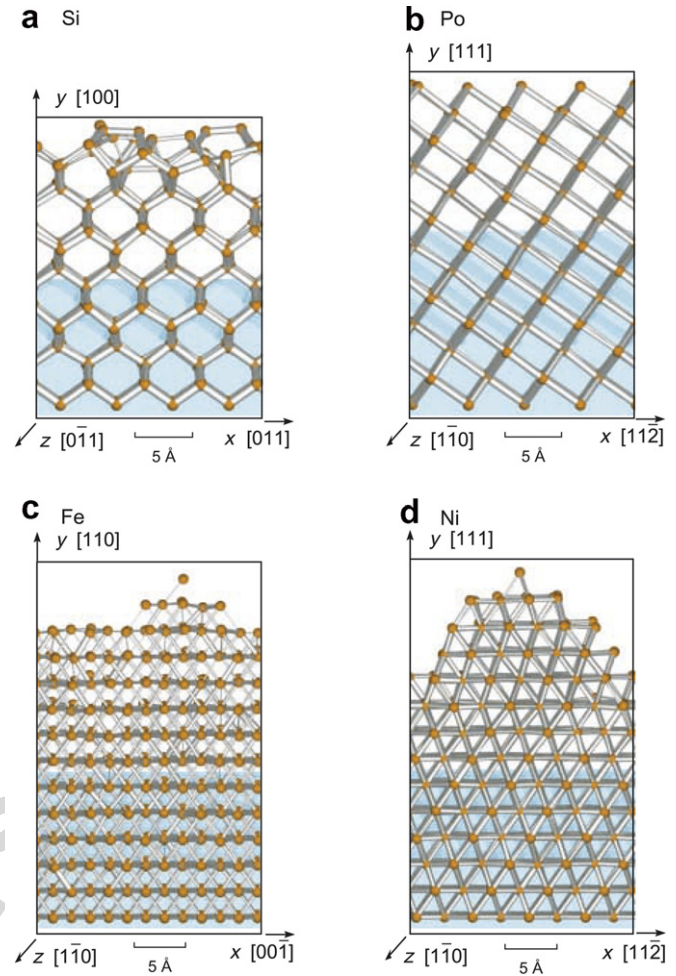


Fig. 2. Atomic configurations for the films deposited at a temperature of 650 K, an adatom incident angle perpendicular to the surface, an adatom remote kinetic energy of 1.0 eV, and a growth rate of 0.5 nm/ns. (a) Si; (b) Po; (c) Fe; and (d) Ni. The substrate regions prior to deposition are shaded.

The Po and Fe surfaces appear to be less rough in Fig. 2(b) and (c). However, more careful examination indicated that there are numerous unfilled lattice sites extending several atomic layers below the surface. Under kinetically constrained conditions (low growth temperature or high deposition rate), these unfilled sites may become buried in the film to form lattice defects such as vacancies.

7. Conclusions

By modifying the potential interaction range and the angular term, elemental SW potentials have been extended to cover the four basic cubic crystals: dc, sc, bcc and fcc. A general procedure to parameterize such a modified SW potential for the growth simulations is demonstrated using the four representative elements, Si, Po, Fe and Ni. The parameterized potential can exactly match the cohesive energy and the lattice constant of the equilibrium phases while predicting higher cohesive energies for any other (metastable) phases. For Si and Po with open equilibrium

structures, the modified SW potential can also exactly match the bulk moduli and closely predict the other elastic constants. For Fe and Ni with densely packed equilibrium structures, the bulk modulus cannot be exactly matched and the other elastic constants are not well reproduced. The SW potentials proposed for Si, Po, Fe, and Ni, can

Eq. (A.2) gives the second relationship between material property (lattice constant) and the free parameters of the potential.

The bulk modulus is related to the second derivative of the cohesive energy through $B = V \cdot d^2E_c/dV^2 = r_1^2 \cdot E_c''/(9V)$. Eq. (A.2) then yields

$$E_c'' = \frac{9 \cdot V \cdot B}{r_1^2} = \frac{A \cdot \sigma}{2 \cdot r_1} \cdot \frac{1}{r_1^2} \sum_{j=1}^n Z_j \cdot \xi_j^2 \cdot \exp\left(\frac{\frac{\sigma}{r_1}}{\xi_j - \frac{r_c}{r_1}}\right) \cdot \left[\frac{-2\xi_j^6 \left(\xi_j - \frac{r_c}{r_1}\right) - \xi_j^6 \left(\frac{\sigma}{r_1}\right) + 20S \left(\xi_j - \frac{r_c}{r_1}\right)^4 \left(\frac{\sigma}{r_1}\right)^3 + 2S\xi_j \left(5\xi_j - \frac{4r_c}{r_1}\right) \left(\xi_j - \frac{r_c}{r_1}\right) \left(\frac{\sigma}{r_1}\right)^4 + S\xi_j^2 \left(\frac{\sigma}{r_1}\right)^5}{\xi_j^6 \cdot \left(\xi_j - \frac{r_c}{r_1}\right)^4} \right] \quad (\text{A.3})$$

be successfully used to study the atomic assembly, structure evolution, and defect formation during the growth of the four elements.

Acknowledgements

We are grateful to the Defense Advanced Research Projects Agency and Office of Naval Research (C. Schwartz and J. Christodoulou, Program managers) for support of this work through grant N00014-03-C-0288.

Appendix A. Material property relations

A.1. A lattice constant, cohesive energy, and bulk modulus

Analytical relations exist between the free parameters of the potential and material properties. In general, the values of atom separation distance, r_1 (or lattice constant, a), cohesive energy, E_c , and elastic bulk modulus, B , determine the function ϕ . The corresponding relations are derived here.

The angular term remains at zero during the hydrostatic strain of the equilibrium crystal. For the pair potential with an interaction up to the n th nearest neighbor shell, the cohesive energy defined by Eq. (1) can be rewritten in a normalized form as

$$E_c = \frac{A}{2} \sum_{j=1}^n Z_j \cdot \exp\left(\frac{\frac{\sigma}{r_1}}{\xi_j - \frac{r_c}{r_1}}\right) \cdot \left[S \left(\frac{\sigma}{r_1}\right)^4 \left(\frac{1}{\xi_j}\right)^4 - 1 \right] \quad (\text{A.1})$$

where j sums over all the neighbor shells. Eq. (A.1) defines a relationship between material property (cohesive energy) and the free parameters of the potential.

Under the equilibrium condition, $E_c' = 0$, we can derive from Eq. (A.1)

$$E_c' = 0 = \frac{A \cdot \sigma}{2 \cdot r_1} \cdot \frac{1}{r_1} \sum_{j=1}^n Z_j \cdot \xi_j \cdot \exp\left(\frac{\frac{\sigma}{r_1}}{\xi_j - \frac{r_c}{r_1}}\right) \times \left[\frac{-4S \cdot \left(\frac{\sigma}{r_1}\right)^3 \cdot \left(\xi_j - \frac{r_c}{r_1}\right)^2 - S \cdot \left(\frac{\sigma}{r_1}\right)^4 \cdot \xi_j + \xi_j^5}{\xi_j^5 \cdot \left(\xi_j - \frac{r_c}{r_1}\right)^2} \right] \quad (\text{A.2})$$

Eq. (A.3) is the third relationship between material property (bulk modulus) and the free parameters of the potential.

Eqs. (A.1)–(A.3) involve four free parameters A , S , σ and r_c . It can be seen that once r_c is chosen, the values of A , S , σ can be solved. Such A , S , σ values predict exactly the target values of the lattice constant, cohesive energy, and bulk modulus.

Appendix B

B.1. Shear moduli

Cubic crystals have three independent elastic constants. In addition to the bulk modulus B , the C_{11} and C_{44} can be chosen to be the remaining two independent elastic constants. Elastic constant C_{ij} is defined as $C_{ij} = \frac{1}{V} \frac{\partial^2 E_c}{\partial \varepsilon_i \partial \varepsilon_j}$, where ε_i , ε_j ($i, j = 1, 2, \dots, 6$) are strains represented by the contracted notation.

To calculate elastic constant C_{ij} , the cohesive energy needs to be expressed as a function of ε_i ($i = 1, 2, \dots, 6$). Assume that a lattice vector from atom i to atom j in an equilibrium crystal is represented by three components $\Delta x_{ij,0}$, $\Delta y_{ij,0}$, $\Delta z_{ij,0}$. The three components become Δx_{ij} , Δy_{ij} , Δz_{ij} after a $\{\varepsilon_1, \varepsilon_2, \dots, \varepsilon_6\}$ strain operation. This strain satisfies:

$$\begin{aligned} \Delta x_{ij} &= \Delta x_{ij,0}(1 + \varepsilon_1) + 0.5\Delta y_{ij,0}\varepsilon_6 + 0.5\Delta z_{ij,0}\varepsilon_5 \\ \Delta y_{ij} &= 0.5\Delta x_{ij,0}\varepsilon_6 + \Delta y_{ij,0}(1 + \varepsilon_2) + 0.5\Delta z_{ij,0}\varepsilon_4 \\ \Delta z_{ij} &= 0.5\Delta x_{ij,0}\varepsilon_5 + 0.5\Delta y_{ij,0}\varepsilon_4 + \Delta z_{ij,0}(1 + \varepsilon_3) \end{aligned} \quad (\text{B.1})$$

The distance between atoms i and j is

$$r_{ij} = \sqrt{\Delta x_{ij}^2 + \Delta y_{ij}^2 + \Delta z_{ij}^2} \quad (\text{B.2})$$

and the bond angle can be calculated as

$$\cos \theta_{jik} = \frac{\Delta x_{ij} \cdot \Delta x_{ik} + \Delta y_{ij} \cdot \Delta y_{ik} + \Delta z_{ij} \cdot \Delta z_{ik}}{r_{ij} \cdot r_{ik}} \quad (\text{B.3})$$

Substitution of Eqs. (B.1)–(B.3) into Eq. (1) then gives an E_c as a function of ε_i ($i = 1, 2, \dots, 6$).

Table B.1
Selected values of F , G , and H for dc, sc, bcc and fcc crystals

Structures	α	F_1	F_2	G_1	G_2	H_1
dc	1	0.22222	2.66667	0.44444	1.63299	4.74074
	4	0.22222	1.33333	0.11111	0.81650	0.79012
sc	1	1.00000	2.00000	0.00000	1.41421	0.00000
	4	0.00000	1.00000	0.50000	0.70711	8.00000
fcc	1	1.00000	2.00000	1.00000	0.00000	28.00000
	4	0.50000	0.00000	0.50000	0.70711	12.00000
bcc	1	0.44444	1.33333	0.88889	0.00000	18.96297
	4	0.44444	0.00000	0.22222	0.57735	3.16049

$$u(r_1) = \sqrt{\frac{V[C_{11}H_1(1) + C_{44}H_1(4)] - r_1^2 \sum_{k=1}^n \phi''(r_k)[F_k(1)H_1(1) + F_k(4)H_1(4)] - r_1 \sum_{k=1}^n \phi'(r_k)[G_k(1)H_1(1) + G_k(4)H_1(4)]}{[H_1(1)^2 + H_1(4)^2]}} \quad (\text{B.8})$$

As described above, the form of the g function for the equilibrium crystal has been designed to satisfy $g(\cos \theta_{jik}) = g'(\cos \theta_{jik}) = 0$ and $g''(\cos \theta_{jik}) = 2$. Under the equilibrium condition ($\varepsilon_1 = \varepsilon_2 = \dots = \varepsilon_6 = 0$), the elastic constant $C_{\alpha\alpha}$ ($\alpha = 1, 2, \dots, 6$) can then be written as

$$\begin{aligned} C_{\alpha\alpha} &= \frac{r_1^2}{V} \sum_{m=1}^n \phi''(r_m) \cdot \frac{1}{2Nr_1^2} \sum_{i=1}^N \sum_{j=i_1(m)}^{i_N(m)} \left(\frac{\partial r_{ij}}{\partial \varepsilon_\alpha} \right)^2 \\ &+ \frac{r_1}{V} \sum_{m=1}^n \phi'(r_m) \cdot \frac{1}{2Nr_1} \sum_{i=1}^N \sum_{j=i_1(m)}^{i_N(m)} \frac{\partial^2 r_{ij}}{\partial \varepsilon_\alpha^2} \\ &+ \frac{[u(r_1)]^2}{V} \cdot \frac{1}{N} \sum_{i=1}^N \sum_{j=i_1(1)}^{i_N(1)} \sum_{\substack{k=i_1(1) \\ k \neq j}}^{i_N(1)} \left(\frac{\partial \cos \theta_{jik}}{\partial \varepsilon_\alpha} \right)^2 \\ &= \frac{r_1^2}{V} \sum_{m=1}^n \phi''(r_m) \cdot F_m(\alpha) + \frac{r_1}{V} \sum_{m=1}^n \phi'(r_m) \cdot G_m(\alpha) \\ &+ \frac{[u(r_1)]^2}{V} \cdot H_1(\alpha) \end{aligned} \quad (\text{B.4})$$

where

$$F_m(\alpha) = \frac{1}{2Nr_1^2} \sum_{i=1}^N \sum_{j=i_1(m)}^{i_N(m)} \left(\frac{\partial r_{ij}}{\partial \varepsilon_\alpha} \right)^2 \quad (\text{B.5})$$

$$G_m(\alpha) = \frac{1}{2Nr_1} \sum_{i=1}^N \sum_{j=i_1(m)}^{i_N(m)} \frac{\partial^2 r_{ij}}{\partial \varepsilon_\alpha^2} \quad (\text{B.6})$$

$$H_1(\alpha) = \frac{1}{N} \sum_{i=1}^N \sum_{j=i_1(1)}^{i_N(1)} \sum_{\substack{k=i_1(1) \\ k \neq j}}^{i_N(1)} \left(\frac{\partial \cos \theta_{jik}}{\partial \varepsilon_\alpha} \right)^2 \quad (\text{B.7})$$

Here we adopt a notation of “ m ” in F_m , G_m , and H_m and “ (m) ” in $i_1(m)$ and $i_N(m)$ to indicate that the neighbors used in the calculation are in the m th nearest neighbor shell. Eq. (B.7) only gives the nearest neighbor shell because only the

nearest neighbors are considered in the angular term. F_m , G_m , and H_m are independent of the lattice constant, and can therefore be viewed as constants for each crystal structure. Selected values of F_m , G_m , and H_m needed for the C_{11} and C_{44} calculations in the present paper are shown in Table B.1 for the four crystals.

Eq. (B.4) can be used to determine $u(r_1)$ by either exactly matching one of the two elastic constants (C_{11} , C_{44}) or minimizing the square deviation of both C_{11} and C_{44} . Using the square deviation minimization approach, we have

Eq. (B.8) gives the fourth relationship between material properties (shear moduli) and the free parameters of the potential. It should be noted that Eq. (B.8) involves three free parameters C , γ , and r_{uc} . As a result, Eq. (B.8) alone does not fully define the parameters even the cutoff distance r_{uc} is chosen. The additional freedom is actually desired as it can be adjusted to ensure that the equilibrium phase indeed has the lowest cohesive energy with respect to other phases.

References

- [1] S.O. Kasap, in: K.T. Kane, C. Fields (Eds.), Principles of Electrical Engineering Materials and Devices, McGraw-Hill, New York, 2000, p. 1.
- [2] S. Strite, H. Morkoc, J. Vac. Sci. Technol. B 10 (1992) 1237.
- [3] S.J. Pearton, J.C. Zolper, R.J. Shul, F. Ren, J. Appl. Phys. 86 (1999) 1.
- [4] I. Akasaki, IPAP Conf. Series 1 (2000) 1.
- [5] D. Wang, C. Nordman, J.M. Daughton, Z. Qian, J. Fink, IEEE Trans. Mag. 40 (2004) 2269.
- [6] J.H. Yu, H.M. Lee, Y. Ando, T. Miyazaki, Appl. Phys. Lett. 82 (2003) 4735.
- [7] R.S. Beech, J. Anderson, J. Daughton, B.A. Everitt, D. Wang, IEEE Trans. Magn. 32 (1996) 4713.
- [8] J.S. Moodera, L.R. Kinder, T.M. Wong, R. Meservey, Phys. Rev. Lett. 74 (1995) 3273.
- [9] K. Shimazawa, J.J. Sun, N. Kasahara, K. Sato, T. Kagami, S. Saruki, O. Redon, Y. Fujita, T. Umehara, J. Syoji, S. Araki, M. Matsuzaki, IEEE Trans. Magn. 37 (2001) 1684.
- [10] M. Tondra, J.M. Daughton, D. Wang, R.S. Beech, A. Fink, J.A. Taylor, J. Appl. Phys. 83 (1998) 6688.
- [11] H.A.M. van den Berg, J. Altmann, L. Bar, G. Gieres, R. Kinder, R. Rupp, M. Vieth, J. Wecker, IEEE Trans. Magn. 35 (1999) 2892.
- [12] M. Durlam, P.J. Naji, A. Omair, M. DeHerrera, J. Calder, J.M. Slaughter, B.N. Engel, N.D. Rizzo, G. Grynkewich, B. Butcher, C. Tracy, K. Smith, K.W. Kyler, J.J. Ren, J.A. Molla, W.A. Feil, R.G. Williams, S. Tehrani, IEEE J. Sol. State Cir. 38 (2003) 769.
- [13] S. Yuasa, T. Nagahama, A. Fukushima, Y. Suzuki, K. Ando, Nat. Mater. 3 (2004) 868.
- [14] X.W. Zhou, H.N.G. Wadley, R.A. Johnson, D.J. Larson, N. Tabat, A. Cerezo, A.K. Petford-Long, G.D.W. Smith, P.H. Clifton, R.L. Martens, T.F. Kelly, Acta Mater. 49 (2001) 4005.
- [15] W. Zou, H.N.G. Wadley, X.W. Zhou, R.A. Johnson, Phys. Rev. B 64 (2001) 174418.

- [16] X.W. Zhou, H.N.G. Wadley, *Phys. Rev. B* 71 (2005) 54418.
- [17] X.W. Zhou, H.N.G. Wadley, *J. Appl. Phys.* 84 (1998) 2301.
- [18] X.W. Zhou, R.A. Johnson, H.N.G. Wadley, *Phys. Rev. B* 69 (2004) 144113.
- [19] M.S. Daw, M.I. Baskes, *Phys. Rev. B* 29 (1984) 6443.
- [20] F.H. Stillinger, T.A. Weber, *Phys. Rev. B* 31 (1985) 5262.
- [21] J. Tersoff, *Phys. Rev. B* 37 (1988) 6991.
- [22] J. Tersoff, *Phys. Rev. B* 39 (1989) 5566.
- [23] J. Tersoff, *Phys. Rev. B* 41 (1990) 3248.
- [24] D.W. Brenner, *Phys. Rev. B* 42 (1990) 9458.
- [25] X.W. Zhou, D.A. Murdick, H.N.G. Wadley, in preparation.
- [26] C.H. Grein, J.P. Faurie, V. Bousquet, E. Tournie, R. Benedek, T. de la Rubia, *J. Cryst. Growth* 178 (1997) 258.
- [27] G.H. Gilmer, C. Roland, *Appl. Phys. Lett.* 65 (1994) 824.
- [28] B. Strickland, C. Roland, *Phys. Rev. B* 51 (1995) 5061.
- [29] H.W. Lu, J.Y. Feng, *Modell. Simul. Mater. Sci. Eng.* 8 (2000) 621.
- [30] J. Nord, K. Albe, P. Erhart, K. Nordlund, *J. Phys. Condens. Matter* 15 (2003) 5649.
- [31] J. Nord, K. Nordlund, J. Keinonen, K. Albe, *Nucl. Instr. Meth. Phys. Res. B* 202 (2003) 93.
- [32] X.W. Zhou, D.A. Murdick, B. Gillespie, H.N.G. Wadley, *Phys. Rev. B* 73 (2006) 45337.
- [33] J. Kioseoglou, H.M. Polatoglou, L. Lympirakis, G. Nouet, P. Komninou, *Comput. Mater. Sci.* 27 (2003) 43.
- [34] X.W. Zhou, H.N.G. Wadley, in preparation.
- [35] CRC Handbook of Chemistry and Physics.
- [36] S.M. Foiles, M.I. Baskes, M.S. Daw, *Phys. Rev. B* 33 (1986) 7983.
- [37] R.E. Kraig, D. Roundy, M.L. Cohen, *Solid State Commun.* 129 (2004) 411.
- [38] D.J. Eaglesham, H.-J. Gossman, M. Cerullo, *Phys. Rev. Lett.* 65 (1990) 1227.
- [39] X.W. Zhou, H.N.G. Wadley, *Acta Mater.* 47 (1999) 1063.